

# NeurInt : Learning to Interpolate through Neural ODEs

Avinandan Bose <sup>\*1</sup>, Aniket Das <sup>\*1</sup>, Yatin Dandi <sup>1</sup>, Piyush Rai <sup>1</sup>

<sup>1</sup>Indian Institute of Technology Kanpur

## Abstract

A wide range of applications require learning image generation models whose latent space effectively captures the high-level factors of variation present in the data distribution. The extent to which a model represents such variations through its latent space can be judged by its ability to interpolate between images smoothly. However, most generative models mapping a fixed prior to the generated images lead to interpolation trajectories lacking smoothness and containing images of reduced quality. In this work, we propose a novel generative model that learns a flexible non-parametric prior over interpolation trajectories, conditioned on a pair of source and target images. Instead of relying on deterministic interpolation methods (such as linear or spherical interpolation in latent space), we devise a framework that learns a distribution of trajectories between two given images using Latent Second-Order Neural Ordinary Differential Equations. Through a hybrid combination of reconstruction and adversarial losses, the generator is trained to map the sampled points from these trajectories to sequences of realistic images that smoothly transition from the source to the target image. Through comprehensive qualitative and quantitative experiments, we demonstrate our approach's effectiveness in generating images of improved quality as well as its ability to learn a diverse distribution over smooth interpolation trajectories for any pair of real source and target images.

## Introduction

In the past few years, deep generative models' incredible success has demonstrated their ability to represent the underlying factors of variations in high dimensional data, such as images via low dimensional latent variables. These factors of variation are commonly visualized by interpolating between images by traversing particular paths in the latent space. Given any two images, it is often desirable to obtain a distribution over various possible trajectories of smooth and realistic image space interpolations. Learning such distribution would allow a more extensive analysis of the factors of variation in data. In this work, we propose an approach that jointly trains an encoder and a generator to successively transform latent vectors on a trajectory to interpolations from a given source to a target image. To flexibly model distributions over trajectories of latent vectors, we parameterize their dynamics in continuous-time using Neural

Ordinary Differential Equations (Chen et al. 2018). We refer to our approach as Neural Interpolation (NeurInt) (Figure 1).

Through comprehensive qualitative and quantitative evaluation on different image datasets, we verify our approach's effectiveness for generating a diverse set of smooth and realistic interpolations and demonstrate its improved generation and reconstruction qualities.

Ideally, we wish every point in the latent space to map to a unique, real image. However, it is unrealistic to expect a model to learn the entire data distribution over infinitely many real images given only a finite dataset (Arora, Risteski, and Zhang 2017). Thus, given any image, we can only expect the model to learn to transform it to neighboring realistic images through suitable incremental changes. In view of this, instead of generating an image from random noise, our approach encourages the model to traverse through realistic images while maintaining smoothness and a net movement towards the target image. By *learning* to interpolate instead of using a deterministic interpolation technique, we allow the model to generate different categories of interpolations for different source and target images. This is achieved by learning a *distribution* over trajectories conditioned on the source and target images, parameterized by second-order Neural ODEs. Leveraging a *data-dependent* latent space distribution, parameterized through Neural ODEs, lends our approach the following major advantages:

- The direct utilization of real images while sampling latent vectors allows our approach to incorporate the benefits of non-parametric approaches, such as the ability to incorporate additional data into the generative model without retraining the parameters.
- The model exhibits the flexibility to learn different latent space distributions depending on the training data's complexity and size.
- The second-order formulation allows our model to map randomly sampled initial velocities from a simple Gaussian prior to a highly expressive class of smooth trajectories corresponding to different vector fields on the data distribution manifold.
- The continuous nature of the ODE further allows us to sample an arbitrary number of points in each trajectory to obtain the desired level of smoothness in the interpolation trajectories where the smoothness is naturally en-

<sup>\*</sup>These authors contributed equally.

forced by the ODE formulation.

- Simultaneously enforcing smoothness and realism of interpolated images prevents the model from simply memorizing training data.
- Since our model’s latent space distribution directly depends on the encoder, we do not require explicit matching of prior and posterior distributions, unlike other encoder-generator based approaches such as VAE (Kingma and Welling 2013) and ALI (Dumoulin et al. 2016)
- Lastly, the computational cost of sampling trajectories can be varied during training and test times by using different discretization schemes depending on the available computational resources.

## Related Work

The progress in the design of latent variable-based deep generative models such as GANs (Goodfellow et al. 2017), VAEs (Kingma and Welling 2013), and normalizing flows (Rezende and Mohamed 2015) in recent years has led to numerous applications. Generative Adversarial Networks (GANs), in particular, have been extensively utilized for image generation (Karras et al. 2017; Brock, Donahue, and Simonyan 2019; Denton et al. 2015; Karras, Laine, and Aila 2019), video generation (Tulyakov et al. 2018; Clark, Donahue, and Simonyan 2019; Dandi et al. 2020), image translation (Isola et al. 2017; Zhu et al. 2017), as well as various other tasks requiring the generation of high-dimensional data. This has also led to vast literature on improving inference (Dumoulin et al. 2016; Dandi et al. 2021; Makhzani et al. 2016; Ulyanov, Vedaldi, and Lempitsky 2018; Mescheder, Nowozin, and Geiger 2017), and training stability (Mescheder, Nowozin, and Geiger 2018; Arjovsky, Chintala, and Bottou 2017) of GANs. However, work on improving the diversity, smoothness, and realism of interpolations has been limited. One of the major reasons for poor interpolation quality is the mismatch between latent vectors’ distributions corresponding to interpolations and the prior distribution used during training. Some recent works have attempted to tackle this mismatch by modifying the prior (White 2016; Leśniak, Sieradzki, and Podolak 2018; Boesen et al. 2017) or using non-parametric priors (Singh et al. 2019). However, unlike our approach which ensures matching image distributions corresponding to entire trajectories with real data distribution, these works only focus on matching the latent space distribution for midpoints of sampled noise vectors. A recent work (Chen et al. 2018) exploited Neural Ordinary Differential Equations’ inherently sequential nature to model continuous time dynamics of time-series data. However, such an approach cannot be directly applied to generating interpolations in the training data. Therefore, we leverage Neural ODEs (Chen et al. 2018) for traversing the latent space while ensuring realism through the use of a discriminator. Our work is also related to but different from Exemplar models (Norouzi, Fleet, and Norouzi 2020) and Kernel Density Estimation (Parzen 1962). While Exemplar based generative models directly utilize the dataset for modeling the latent space distribution, each generated image in such models is obtained by modifying only one randomly

sampled image. Our approach instead can find points on image space between any arbitrarily pair of images, enabling it to capture the full diversity of image data manifolds for both generation as well as interpolation. Moreover, our GAN based formulation allows directly matching the image distribution of trajectories of interpolants with the real data distribution. This obviates the need of utilizing a nearest-neighbour based approximation of a closed form non-parametric distribution in the latent space. By directly enforcing smoothness and realism of interpolated images, our approach also prevents memorization of training data without utilizing regularization (Norouzi, Fleet, and Norouzi 2020) or pseudo-inputs (Tomczak and Welling 2018a).

The set of source and target images in our model can also be interpreted as a form of external memory, which has been shown to improve generation quality in several works (Bornschein et al. 2017; Guu et al. 2018; Hoffman and Johnson 2016; Tomczak and Welling 2018b; Khandelwal et al. 2019; Li, Zhu, and Zhang 2016).

The use of Neural ODEs in our approach is inspired by their recent application to a variety of domains. On account of their continuous-time formalism, Neural ODEs, unlike traditional discrete-time sequence models, are capable of handling non-uniformly sampled temporal data with no additional overhead. As a result, they are inherently suited to applications, such as time-series forecasting (Chen et al. 2018; Rubanova, Chen, and Duvenaud 2019) and deep generative models of continuous-time data (Chen et al. 2018; Yildiz, Heinonen, and Lahdesmaki 2019), moreover, due to their smoothness and invertibility properties (Zhang et al. 2020), Neural ODEs also find application in density estimation and variational inference as Continuous Normalizing Flows. (Chen et al. 2018; Grathwohl et al. 2018)

## Background

Since our approach is based on neural ODEs, in this section, we briefly review neural ODEs and second-order neural ODEs, and approaches to solve these.

**Neural ODEs** Various deep learning architectures, such as Residual Networks, RNNs and Normalizing Flows can be formulated as a discrete sequence of additive transformations on a state variable  $\mathbf{z}_t$

$$\mathbf{z}_{t+1} = \mathbf{z}_t + f_\theta(\mathbf{z}_t)$$

where the transition function  $f_\theta$  is modelled by a neural network. The above operation can be identified as a unit time-step Euler discretization of a continuous-time system. Hence, taking the continuous limit of the additive transition, we obtain a First-Order ODE system for  $\mathbf{z}_t$

$$\frac{d\mathbf{z}_t}{dt} = f_\theta(\mathbf{z}_t)$$

The neural network  $f_\theta$ , which was previously the discrete-time transition function, now becomes the vector field for the First-Order ODE governing the time evolution of the state  $\mathbf{z}_t$ . This framework is known as Neural Ordinary Differential Equations (Chen et al. 2018). The value of the state  $\mathbf{z}_t$  at any given time, as a function of the input or initial state  $\mathbf{z}_0$ , is

obtained by solving the Initial Value Problem (IVP)

$$\mathbf{z}_t = \mathbf{z}_0 + \int_0^t f_\theta(\mathbf{z}_\tau) d\tau$$

While exact solution is infeasible in most cases, the IVP can be approximately solved with high accuracy using Numerical ODE solvers such as Runge Kutta (RK4) and Dormand Price (DOPRI5). Gradients can either be obtained by ordinary backpropagation or by using the Adjoint State Method, (Chen et al. 2018) which allows gradient computation without backpropagating through ODE solver operations.

**Second-Order Neural ODEs** Despite the impressive continuous-time modeling capabilities of (First-Order) Neural ODEs, there exist various classes of phenomena (e.g. Harmonic and Van der Pol oscillators) whose latent dynamics cannot be modeled by First-Order ODE systems. This motivates the use of Second-Order Neural ODEs (Yildiz, Heinonen, and Lahdesmaki 2019), a framework where the time evolution of the state variable  $\mathbf{z}_t$  is governed by

$$\frac{d^2 \mathbf{z}_t}{dt^2} = f_\theta(\mathbf{z}_t, \dot{\mathbf{z}}_t)$$

Analogous to First-Order Neural ODEs, the vector field  $f_\theta(\mathbf{z}_t, \dot{\mathbf{z}}_t)$  is modelled by a Neural Network. However, a key difference lies in the fact that the vector field is a function of the state  $\mathbf{z}_t$  as well as the state differential  $\dot{\mathbf{z}}_t = \frac{d\mathbf{z}_t}{dt}$ . This feature allows Second-Order Neural ODEs to model much more complex dynamical systems that cannot be modeled by First-Order Neural ODEs. Moreover, Second-Order Neural ODEs have much better smoothness properties as they ensure the continuity of the second derivative of state  $\frac{d^2 \mathbf{z}_t}{dt^2}$ .

To facilitate numerical integration, the Second-Order Neural ODE is reduced to an equivalent Coupled First-Order ODE system by introducing an auxiliary state variable  $\mathbf{v}_t$  (often named velocity) as follows.

$$\begin{cases} \frac{d\mathbf{z}_t}{dt} = \mathbf{v}_t \\ \frac{d\mathbf{v}_t}{dt} = f_\theta(\mathbf{z}_t, \mathbf{v}_t) \end{cases}$$

This ODE system can be interpreted as a First-Order Neural ODE for the augmented state  $[\mathbf{z}_t, \mathbf{v}_t]^T$ . Consequently, it can be transformed into an Initial Value Problem (IVP)

$$\begin{bmatrix} \mathbf{z}_t \\ \mathbf{v}_t \end{bmatrix} = \begin{bmatrix} \mathbf{z}_0 \\ \mathbf{v}_0 \end{bmatrix} + \int_0^t \begin{bmatrix} \mathbf{v}_\tau \\ f_\theta(\mathbf{z}_\tau, \mathbf{v}_\tau) \end{bmatrix} d\tau$$

which, can be solved by Numerical ODE solvers. As discussed earlier, gradient computation can be performed either by backpropagating through the ODE solver’s operations or by using the Adjoint State Method (Chen et al. 2018).

## Neural Interpolation (NeurInt)

Our approach, NeurInt, models a distribution over smooth continuous-time interpolation curves  $\tilde{\mathbf{x}}_t : [0, T] \rightarrow \mathcal{X}$  (where  $T \in \mathbb{R}^+$  and  $\mathcal{X}$  represents the image manifold) which start from a given source image  $\mathbf{x}_S$  and end at a target image  $\mathbf{x}_T$ . The source and target are sampled from a fixed

---

### Algorithm 1: NeurInt: Generation

---

**Input:** Source Image  $\mathbf{x}_S$ , Target Image  $\mathbf{x}_T$  and Integration time  $T$

**Output:** Continuous-time Interpolation Curve  $\tilde{\mathbf{x}}_t : [0, T] \rightarrow \mathcal{X}$

- 1 Set initial latent  $\mathbf{z}_0$  of latent space trajectory  $\mathbf{z}_0 := E(\mathbf{x}_S)$
  - 2 Sample Initial Velocity  $\epsilon \sim \mathcal{N}(0, \mathbf{I})$ ;  $\mathbf{v}_0 = \mu_v(\mathbf{z}_0, E(\mathbf{x}_T)) + \epsilon \odot \sigma_v(\mathbf{z}_0, E(\mathbf{x}_T))$ ;
  - 3 Solve ODE System for  $\mathbf{z}_t : [0, T] \rightarrow \mathcal{X}$ ;  $\frac{d^2 \mathbf{z}_t}{dt^2} = f(\mathbf{z}_t, \dot{\mathbf{z}}_t) \quad \dot{\mathbf{z}}_0 = \mathbf{v}_0$ ;
  - 4 Generate Interpolation Curve  $\tilde{\mathbf{x}}_t : [0, T] \rightarrow \mathcal{X}$ ;  $\tilde{\mathbf{x}}_t = G(\mathbf{z}_t)$ ;
- 

dataset defined by  $p_{data}(\mathbf{x})$ . Samples from the generative model of NeurInt can be drawn by a two stage process, by first sampling from the distribution of interpolation curves, and then evaluating the sampled interpolation curve at random time-points.

Similar to other latent variable-based generative models, we define the generated data distribution  $p(\mathbf{x})$  as the distribution obtained by transforming a latent space distribution  $p(\mathbf{z})$  through a generator  $\mathcal{G}$ . However, unlike generative models with fixed parametric priors, the latent space distribution  $p(\mathbf{z})$  in our model is defined through a distribution over latent trajectories  $\mathbf{z}_t : [0, T] \rightarrow \mathcal{Z}$  conditioned over source and target images. Time evolution of these trajectories is governed by a Second-Order Neural ODE of the form

$$\frac{d^2 \mathbf{z}_t}{dt^2} = f(\mathbf{z}_t, \dot{\mathbf{z}}_t)$$

In order to ensure that all image interpolation curves that are conditioned on  $\mathbf{x}_S$  and  $\mathbf{x}_T$  begin at the source, a *Position Encoder*  $E$  is used to project  $\mathbf{x}_S$  to  $\mathcal{Z}$ , and the initial position  $\mathbf{z}_0$  of the trajectory is set to  $E(\mathbf{x}_S)$ . The distribution over latent trajectories is defined by placing a data dependent prior on the initial velocity  $\mathbf{v}_0$  or  $\dot{\mathbf{z}}_0$ . For our modeling purposes, we choose the prior  $p(\mathbf{v}_0 | \mathbf{x}_S, \mathbf{x}_T)$  to be a Diagonal Gaussian whose parameters are given by the *Velocity Encoder*  $\mathcal{V} = (\mu_v, \sigma_v)$ . We observe in our experiments that imposing such a prior on the initial velocity leads to a diverse distribution over interpolation trajectories even for a fixed pair of source and target images.

Sampling a latent trajectory  $\mathbf{z}_t$  hence consists of evaluating  $\mathbf{z}_0$  and sampling an initial velocity  $\mathbf{v}_0$  from the data dependent prior. This fixes the Initial Value Problem (IVP) for the trajectory, which can now be obtained by (numerical) integration of the ODE system. The true image space curve  $\tilde{\mathbf{x}}_t$  is then obtained by transforming  $\mathbf{z}_t$  using the generator, and can be sampled at arbitrarily chosen time-points in the range  $[0, T]$  to produce image samples. The specifics of the generative process is described in Algorithm 1.

The learning objective of the model ensures that a given image space curve  $\tilde{\mathbf{x}}_t$  which is conditioned on a source target pair  $(\mathbf{x}_S, \mathbf{x}_T)$  begins at the source and ends at the target.

---

**Algorithm 2: NeurInt: Training**

---

**Input:** Dataset  $P_{\text{data}}(\mathbf{x})$ , Hyperparameter  $\lambda$  and Integration time  $T$

- 1 Sample  $\mathbf{x}_S$  and  $\mathbf{x}_T$  from the dataset  $P_{\text{data}}(\mathbf{x})$
  - 2 Set initial latent  $\mathbf{z}_0$  of trajectory  
 $\mathbf{z}_0 := E(\mathbf{x}_S)$
  - 3 Sample Initial Velocity ::  
 $\epsilon \sim \mathcal{N}(0, \mathbf{I})$ ;  
 $\mathbf{v}_0 = \mu_v(\mathbf{z}_0, E(\mathbf{x}_T)) + \epsilon \odot \sigma_v(\mathbf{z}_0, E(\mathbf{x}_T))$ ;
  - 4 Solve ODE System for for  $z_t : [0, T] \rightarrow \mathcal{X}$ ;  
 $\frac{d^2 \mathbf{z}_t}{dt^2} = f(\mathbf{z}_t, \dot{\mathbf{z}}_t) \quad \dot{\mathbf{z}}_0 = \mathbf{v}_0$ ;
  - 5 Compute Reconstruction Loss;  
 $\mathcal{L}_{\text{AE}} = \|\mathbf{x}_S - G(\mathbf{z}_0)\|_2^2 + \|\mathbf{x}_T - G(\mathbf{z}_T)\|_2^2$ ;
  - 6 Sample  $t_1, \dots, t_N$  from Uniform  $(0, T)$  without replacement ;
  - 7 Sample  $\mathbf{x}_1, \dots, \mathbf{x}_N$  from dataset;  
 $\mathcal{L}_{\text{GAN}} = \sum_{i=1}^N \log(D(\mathbf{x}_i)) + \log(1 - D(G(\mathbf{z}_{t_i})))$  ;
  - 8 Optimize the minimax game with (Stochastic) Gradient Descent Ascent;  
$$\min_{\mathcal{G}, \mathcal{E}, \mu_v, \sigma_v, f} \max_D \mathcal{L}_{\text{GAN}} + \lambda \mathcal{L}_{\text{AE}} ;$$
- 

This is ensured by a pixel-MSE based reconstruction objective  $\mathcal{L}_{\text{AE}}$  that matches  $\tilde{\mathbf{x}}_0$  to  $\mathbf{x}_S$  and  $\tilde{\mathbf{x}}_T$  to  $\mathbf{x}_T$ . The realism and diversity of interpolation curves is ensured via Adversarial Learning. We use the Generative Adversarial Network to jointly train a critic  $D : \mathcal{X} \rightarrow [0, 1]$  which discriminates real samples drawn from the data distribution against evaluations of the interpolation trajectory at randomly sampled time-points. Learning is then formulated as a minimax game where the critic  $D$  plays against the encoders  $E$  and  $\mathcal{V}$ , generator  $G$  and the Neural ODE  $f$ . The value function of the game is taken to be a weighted combination of the reconstruction and adversarial objectives. The entire training process is described in Algorithm 2.

We find that the combination of adversarial and reconstruction losses, along with the smoothness properties of Second-Order Neural ODEs is sufficient to ensure that each interpolation curve exhibits a smooth variation from source to target, while simultaneously having image samples of high quality and diversity at each time-point. The non-parametric data dependent prior also allows our model to perform well when conditioned on unseen data, and leads to noticeable improvement in quality when new unseen data is incorporated at test time, without any retraining. These properties, as well as other attributes of the model are thoroughly investigated both qualitatively and quantitatively in the subsequent section.

## Experiments

We benchmark NeurInt, which leverages learnable interpolation trajectories, against the interpolations generated by the Spherical (SLERP) and Linear Interpolations (LERP) on two base generative models, Progressive GAN (PGAN)

(Karras et al. 2017) and Adversarially Learned Autoencoder (ALI) (Dumoulin et al. 2016), on the Street View House Numbers (SVHN) (Netzer et al. 2011) and CelebA (Liu et al. 2015) datasets. To maintain uniformity, the architecture of the Generator and Discriminator for all three models, and that of the Encoder for ALI and NeurInt resemble a standard Progressive GAN. The Neural ODE component of NeurInt uses a Runge Kutta (RK4) integrator with 32 integration timesteps and a total integration time of 1 second ( $T = 1$ ). Further details regarding our architectural choices and hyperparameter selection are described in the Appendix. To evaluate our approach’s interpolation capabilities compared to the baselines, we project the source and target images in the latent space of the respective models, and compare the continuous-time learned interpolations of NeurInt against the interpolations generated by SLERP and LERP for each of the baseline generative models. For NeurInt and ALI, projecting the image to an encoding space is trivial since both the models jointly learn an encoder from the image space to the latent space. However, since PGAN lacks any such means of projection, we train an encoder  $E_P$  that learns to project images onto the trained Progressive GAN latent space. The architecture of  $E_P$  is the same as that of the encoder  $E$  used by NeurInt and it is trained by minimizing a pixel-wise MSE loss and the encoder is progressively grown to maintain consistency.

### Sample Quality, Diversity & Incorporating Unseen Data

We quantitatively assess the generation and interpolation quality for NeurInt and our baselines using Frechet Inception Distance (FID) (Heusel et al. 2017), a standard evaluation metric for GANs, and present the results in Table 1. We randomly select 5000 pairs of source-target images from a support distribution. For NeurInt we generate interpolation trajectories for each pair and randomly sample two intermediate interpolants from each trajectory. For the PGAN and ALI baselines, we project each source-target pair into the latent space, and then generate trajectories using Spherical and Linear Interpolation. The FIDs so obtained are listed under LERP and SLERP in Table 1. To decouple the evaluation of interpolation quality from that of sample generation, we also evaluate the FID of the baselines using samples drawn from their true generative model (listed as PGAN-PRIOR and ALI-PRIOR in Table 1), by sampling a latent code from their respective priors.

Since our approach models distribution over trajectories conditioned on source and target images, the generated data distribution can be flexibly varied by modifying the distribution of source and target images. This allows the trained model to improve the generated data’s diversity without retraining the parameters by incorporating additional data into the set of source and target images. This is unlike the models based on fixed parametric priors, which require retraining on new data to modify the generated data distribution. We repeat the evaluation by varying the support across 3 different distributions, namely the Train Set, the Test Set, as well as the Train and Test set combined. As demonstrated through the results in Table 1, utilizing additional data from the test set leads to improvement in FID scores. Our model’s ability to interpolate on test data also demonstrates its ability to



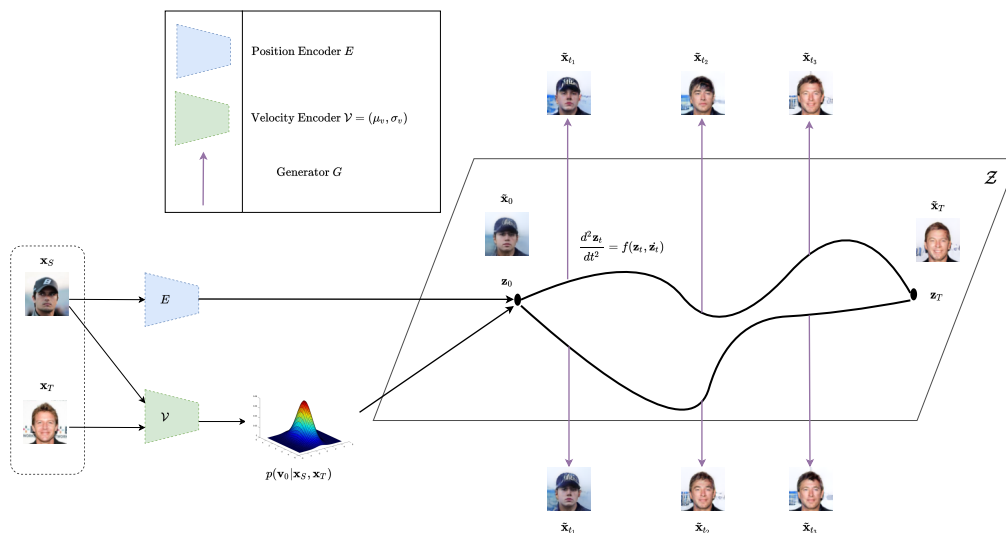


Figure 1: Generative Model of NeurInt. The deterministic position encoder  $E$  sets the initial value of the latent trajectory by projecting the source image  $x_S$  to the latent space, whereas the stochastic velocity encoder  $\mathcal{V}$  inputs the source  $x_S$  and target  $x_T$ , and outputs the parameters of a Diagonal Gaussian distribution over the initial velocity. This induces a distribution over continuous-time latent interpolation trajectories  $z_t$  whose time evolution is governed by the Second-Order Neural ODE. The continuous-time interpolation curve  $\tilde{x}_t$  is generated by mapping  $z_t$  to the image manifold using the Generator  $G$

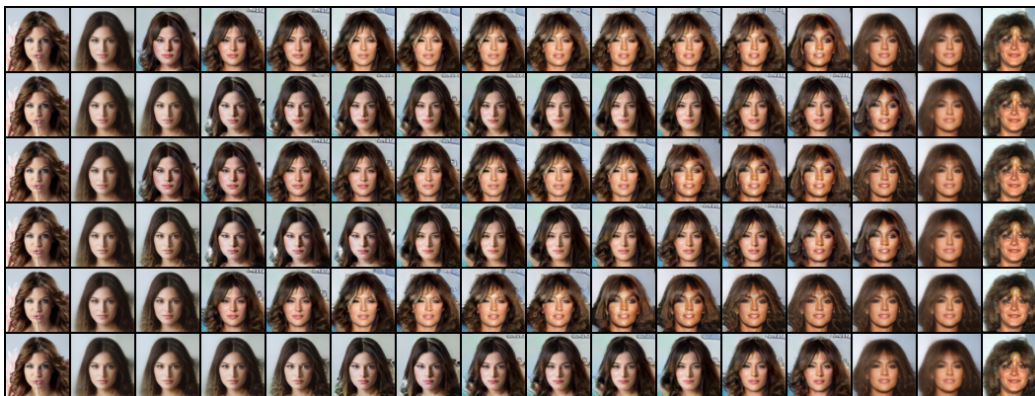


Figure 2: Interpolations upon choosing different initial random velocities for the trajectory, demonstrating the model’s ability to learn a distribution of trajectories, of which the above are six randomly sampled draws. Each row is an interpolation between the real images on the first and last columns.

model the entire image data manifold rather than overfitting on training images.

We note, that across all supports and configurations, NeurInt significantly outperforms all variants of our baselines, quantitatively establishing the superiority of our model in generation and interpolation. This is also qualitatively reflected in Figures 2, 3 and 4, where NeurInt visibly surpasses our baselines. More such samples are presented in the Appendix.

**Improved Representation Learning** We evaluate the representation learning capabilities of NeurInt and our baselines by training a linear SVM model on the feature vectors obtained by concatenating the output layer and the last hidden layer of the encoder for 60,000 class balanced labeled images from the training set of the SVHN dataset. We hold out 10,000 labeled images from the training set as a validation set to tune hyper-parameters of the SVM model. We report the average test misclassification error for 10 different SVM

Table 1: FID scores ( $\downarrow$ ) across various supports & sampling methods.

SUPPORT	DATASET	METHOD	PGAN	ALI	NEURINT
TRAIN SET	SVHN	PRIOR	17.05	46.45	
		LERP	25.23	36.59	<b>6.45</b>
		SLERP	25.43	36.52	
	CELEBA	PRIOR	11.57	19.24	
		LERP	36.28	24.21	<b>10.23</b>
		SLERP	36.45	24.25	
TEST SET	SVHN	PRIOR	17.05	46.45	
		LERP	29.53	37.61	<b>6.82</b>
		SLERP	30.06	37.17	
	CELEBA	PRIOR	11.57	19.24	
		LERP	35.94	23.78	<b>10.37</b>
		SLERP	36.63	23.38	
TRAIN & TEST SET	SVHN	PRIOR	17.05	46.45	
		LERP	24.74	37.57	<b>6.24</b>
		SLERP	25.31	37.04	
	CELEBA	PRIOR	11.57	19.24	
		LERP	36.27	23.77	<b>10.17</b>
		SLERP	36.43	23.95	

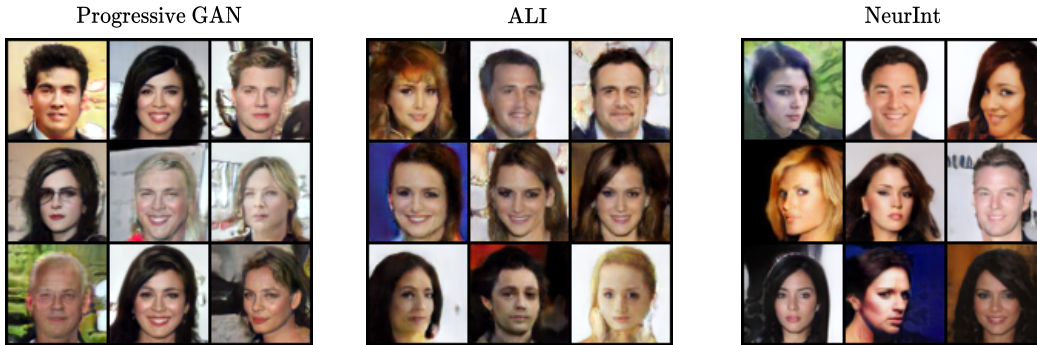


Figure 3: Uncurated samples from Progressive GAN (left), ALI (middle) and NeurInt (right) trained on the CelebA dataset. Samples from Progressive GAN and ALI are drawn from their true prior distribution whereas samples from NeurInt are drawn by first generating continuous-time trajectories and then evaluating them at random intermediate points.

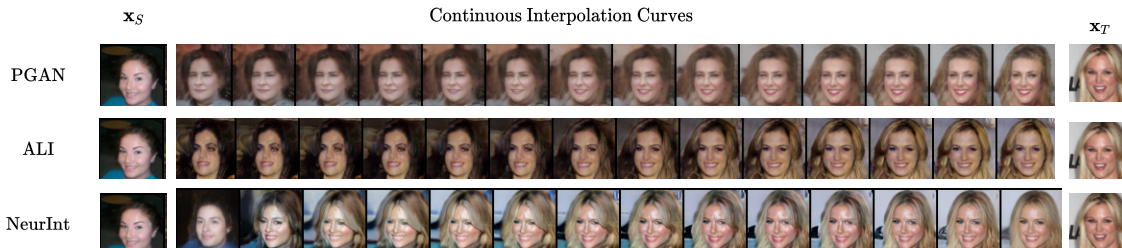


Figure 4: Example Interpolations on CelebA for Top : PGAN, Middle : ALI, Bottom : NeurInt. The first and last columns contain the source and target images respectively

Table 2: Misclassification rate ( $\downarrow$ ) on the test set of SVHN demonstrating the usefulness of learned representations.

Model	Misc rate (%)
PGAN	0.3254 $\pm$ 0.0024
ALI	0.2848 $\pm$ 0.0840
NeurInt	<b>0.2647 <math>\pm</math> 0.0018</b>

models trained on different random 60,000 example training sets. Our results are reported in Table 2.

**Varying ODE Solver Configuration** The Second-Order Neural ODE formulation of NeurInt allows it to interpolate in continuous time. This imparts our approach the flexibility of varying the the level of discretization (number of time-steps) as well as the ODE solver at test time. We validate this by generating trajectories while reducing the number of integrator steps from 32 to 12 in steps of 4 for both RK4 and Euler algorithms. For a fair comparison, we correspondingly vary the time-resolution of the LERP and SLERP interpolators of our baselines and benchmark the models using the FID metric. The results are presented in Table 3 We observe that even at very low integration time-steps, the RK4 variant of NeurInt consistently outperforms the baselines. The same does not hold true for the Euler integrator for very low timesteps, which could be attributed to the inherent coarseness and piecewise linear nature of the Euler Integrator. The discretization invariance of NeurInt has immense practical utility, as it allows us to train the model at a very fine time resolution on a powerful hardware configuration, while deploying it at test time on less powerful hardware by reducing

the accuracy and integrator timesteps of the solver. We also report the time taken for generating the latent interpolants in Table 4 for NeurInt as well as LERP and SLERP in PGAN. We note that RK4, despite using four intermediate increments per solver step, is consistently faster than SLERP.

Table 3: FID scores ( $\downarrow$ ) on varying the solver and timesteps.

Steps	NeurInt		PGAN		ALI	
	RK4	Euler	LERP	SLERP	LERP	SLERP
12	11.17	14.39	36.62	36.82	23.95	24.15
16	11.03	12.99	37.03	36.86	24.35	24.32
20	10.63	12.23	36.00	36.73	24.18	24.26
24	10.47	11.90	36.49	36.85	24.24	24.26
28	10.43	11.23	36.29	37.25	24.04	24.12
32	10.37	10.94	35.94	36.63	23.78	23.38

Table 4: Interpolant generation time (in sec) vs step-size on CelebA averaged over 10 runs on 64000 images

Steps	NeurInt		PGAN	
	RK4	Euler	LERP	SLERP
12	27.48 $\pm$ 0.2	6.31 $\pm$ 0.1	3.76 $\pm$ 0.1	43.64 $\pm$ 0.2
16	33.59 $\pm$ 0.2	10.80 $\pm$ 0.2	6.61 $\pm$ 0.1	49.41 $\pm$ 0.2
20	41.55 $\pm$ 0.2	15.47 $\pm$ 0.3	12.96 $\pm$ 0.2	60.19 $\pm$ 0.2
24	49.85 $\pm$ 0.2	23.84 $\pm$ 0.1	20.81 $\pm$ 0.2	79.69 $\pm$ 0.4
28	58.54 $\pm$ 0.3	33.94 $\pm$ 0.1	40.74 $\pm$ 0.2	113.87 $\pm$ 0.3
32	62.23 $\pm$ 0.2	40.75 $\pm$ 0.2	54.11 $\pm$ 0.2	119.43 $\pm$ 0.1

**Learning a Distribution of Trajectories** To assess the diversity of the interpolation trajectories resulting from the distribution modeled by NeurInt, we generate different trajectories by fixing a source-target pair, drawing multiple

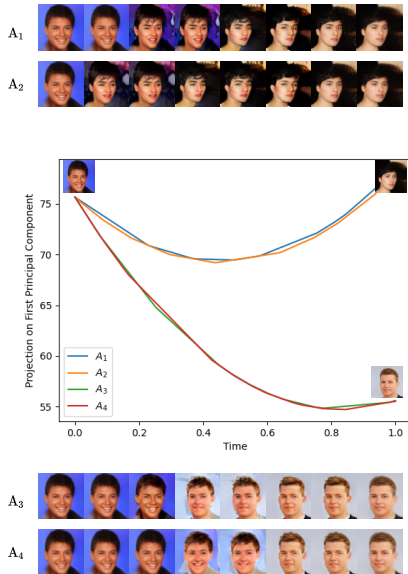


Figure 5: NeurInt learning a distribution of trajectories for interpolation. The top two rows represent samples on the trajectories  $A_1$  and  $A_2$ , while the bottom two rows represent samples on trajectories  $A_3$  and  $A_4$ .

samples of  $\mathbf{v}_0$  conditioned on this fixed source-target pair and generating the corresponding interpolation trajectories. As observed in Rows  $A_1$  and  $A_2$  of Figure 5, the sampled trajectories show noticeable variation in the intermediate interpolants but successfully converge to the same target, as desired. To further emphasise on this variation, we repeat the process by using the same source as Rows  $A_1$  and  $A_2$  but using a different target image as shown in Rows  $A_3$  and  $A_4$ . To visualize these variations in the encoding space, we plot the first Principal Component of each row of Figure 5 over time. It is observed in the plot (Figure 5) that the PCA (F.R.S. 1901) curves of trajectories  $A_1$  and  $A_2$ , starting from the same source, deviate from one another in the middle, thereby reflecting the variety of intermediate interpolants, and towards the end, converge very close to each other, in the neighborhood of the target. The same phenomenon is observed for  $A_3$  and  $A_4$ , whose PCA curves deviate significantly from  $A_1$  and  $A_2$ , on account of having a different target. Furthermore, the PCA curves’ curvature and smoothness confirm that NeurInt truly captures a distribution of smooth and non-linear interpolation trajectories.

**Ablation Study** NeurInt introduces two major modifications to the traditional latent variable based generative modeling:

- A mechanism to smoothly interpolate on the latent space through the use of second-order Neural ODEs.
- A non-parametric data-dependent prior on the latent space obtained by conditioning the generated images on the randomly sampled source and target images.

To evaluate the benefits of jointly incorporating the above two modifications, we perform an ablation experiment where we train the generative model to map images from a fixed latent space prior using the original Generative Adver-

Table 5: FID scores ( $\downarrow$ ) on the CelebA Dataset.

METHOD	PGAN	ALI	NEURINT	NEURINT-PT
PRIOR	11.57	19.24		
LERP	36.28	24.21	<b>10.23</b>	16.94
SLERP	36.45	24.25		

Table 6: FID scores ( $\downarrow$ ) on CelebA dataset by varying Interpolation Method.

Model	FID
NeurInt	<b>10.22 <math>\pm</math> 0.082</b>
LERPInt (LERP in Algorithm 2 Step 4)	16.5 $\pm$ 0.083
SLERPInt (SLERP in Algorithm 2 Step 4)	13.2 $\pm$ 0.077
1 <sup>st</sup> Order NeurInt I ( $\frac{d\mathbf{z}_t}{dt} = f(\mathbf{z}_t)$ )	24.5 $\pm$ 0.072
1 <sup>st</sup> Order NeurInt II ( $\frac{d\mathbf{z}_t}{dt} = f(\mathbf{z}_t, \mathbf{z}_C)$ )	13.5 $\pm$ 0.091

sarial Networks framework and subsequently utilize a Neural ODE network to learn realistic interpolation trajectories on the fixed latent space.

As elucidated by the results in Table 5, while utilizing a Neural ODE to learn interpolation trajectories leads to improvements in quality and diversity over deterministic interpolation methods like LERP and SLERP, it does not improve the overall image generation quality since the generator does not benefit from the training of the interpolator. Jointly training the generator and the interpolator using NeurInt leads to improvements in the smoothness, diversity, and realism of the interpolation trajectories. Moreover, the FID scores’ significant improvements due to joint training further demonstrate NeurInt’s ability to be used for image generation besides interpolation.

**Choice of using a 2<sup>nd</sup> Order ODE** Free initial velocity parameter in 2<sup>nd</sup> Order ODE allows us to parameterize a trajectory distribution for every source target pair. Such a parameter is absent in fixed interpolation schemes and 1<sup>st</sup> Order ODEs of the form  $\frac{d\mathbf{z}_t}{dt} = f(\mathbf{z}_t)$ . Hence, using LERP, SLERP or a 1<sup>st</sup> Order ODE in Algo. 2 Step 4 would prevent us from learning a trajectory distribution for a source-target pair, since such approaches uniquely fix a trajectory given two endpoints. We quantitatively justify our choice by training models that replace Step 4 of Algo. 2 with LERP, SLERP and two 1<sup>st</sup> Order ODEs, namely  $\frac{d\mathbf{z}_t}{dt} = f(\mathbf{z}_t)$  and  $\frac{d\mathbf{z}_t}{dt} = f(\mathbf{z}_t, \mathbf{z}_C)$  where  $\mathbf{z}_C \sim \mathcal{N}(\mu_v(\mathbf{z}_0, E(\mathbf{x}_T)), \sigma_v(\mathbf{z}_0, E(\mathbf{x}_T))^2 \mathbf{I})$ . As shown by FID scores in Table 6, NeurInt outperforms these models.

## Conclusion

In this paper, we proposed a novel generative model which, instead of generating images from a fixed prior, models a flexible distribution of interpolation trajectories conditioned over a source image and a target image using Probabilistic Second-Order Neural ODEs. Thorough qualitative and quantitative evaluation on both the SVHN and CelebA datasets, we establish the superiority of the proposed modeling technique in both generation and interpolation over the respective baselines.

## References

- Arjovsky, M.; Chintala, S.; and Bottou, L. 2017. Wasserstein Generative Adversarial Networks. In *Proceedings of the 34th International Conference on Machine Learning*, volume 70 of *Proceedings of Machine Learning Research*, 214–223. International Convention Centre, Sydney, Australia: PMLR.
- Arora, S.; Risteski, A.; and Zhang, Y. 2017. Theoretical limitations of Encoder-Decoder GAN architectures. *arXiv preprint arXiv:1711.02651*.
- Boesen, A.; Larsen, L.; Sønderby, S. K.; and Winther, O. 2017. Autoencoding beyond pixels using a learned similarity metric. In *CoRR*, abs/1512.09300.
- Bornschein, J.; Mnih, A.; Zoran, D.; and Rezende, D. J. 2017. Variational memory addressing in generative models. *arXiv preprint arXiv:1709.07116*.
- Brock, A.; Donahue, J.; and Simonyan, K. 2019. Large Scale GAN Training for High Fidelity Natural Image Synthesis. In *7th International Conference on Learning Representations, ICLR 2019, New Orleans, LA, USA, May 6-9, 2019*. OpenReview.net.
- Chen, R. T.; Rubanova, Y.; Bettencourt, J.; and Duvenaud, D. K. 2018. Neural ordinary differential equations. In *Advances in neural information processing systems*, 6571–6583.
- Clark, A.; Donahue, J.; and Simonyan, K. 2019. Adversarial video generation on complex datasets. *arXiv preprint arXiv:1907.06571*.
- Dandi, Y.; Bharadhwaj, H.; Kumar, A.; and Rai, P. 2021. Generalized Adversarially Learned Inference. In *AAAI*.
- Dandi, Y.; Das, A.; Singhal, S.; Nambodiri, V.; and Rai, P. 2020. Jointly trained image and video generation using residual vectors. In *Proceedings - 2020 IEEE Winter Conference on Applications of Computer Vision, WACV 2020*.
- Denton, E.; Chintala, S.; Szlam, A.; and Fergus, R. 2015. Deep generative image models using a laplacian pyramid of adversarial networks. *arXiv preprint arXiv:1506.05751*.
- Dumoulin, V.; Belghazi, I.; Poole, B.; Mastropietro, O.; Lamb, A.; Arjovsky, M.; and Courville, A. 2016. Adversarially learned inference. *arXiv preprint arXiv:1606.00704*.
- F.R.S., K. P. 1901. LIII. On lines and planes of closest fit to systems of points in space. *The London, Edinburgh, and Dublin Philosophical Magazine and Journal of Science*, 2(11): 559–572.
- Goodfellow, I. J.; Pouget-Abadie, J.; Mirza, M.; Xu, B.; Warde-Farley, D.; Ozair, S.; Courville, A.; and Bengio, Y. 2017. Generative Adversarial Networks. In *Advances in Neural Information Processing Systems, 2014*.
- Grathwohl, W.; Chen, R. T.; Bettencourt, J.; Sutskever, I.; and Duvenaud, D. 2018. Ffjord: Free-form continuous dynamics for scalable reversible generative models. *arXiv preprint arXiv:1810.01367*.
- Guu, K.; Hashimoto, T. B.; Oren, Y.; and Liang, P. 2018. Generating sentences by editing prototypes. *Transactions of the Association for Computational Linguistics*, 6: 437–450.
- Heusel, M.; Ramsauer, H.; Unterthiner, T.; Nessler, B.; and Hochreiter, S. 2017. Gans trained by a two time-scale update rule converge to a local nash equilibrium. *arXiv preprint arXiv:1706.08500*.
- Hoffman, M. D.; and Johnson, M. J. 2016. Elbo surgery: yet another way to carve up the variational evidence lower bound. In *Workshop in Advances in Approximate Bayesian Inference, NIPS*, volume 1, 2.
- Isola, P.; Zhu, J.-Y.; Zhou, T.; and Efros, A. A. 2017. Image-to-Image Translation with Conditional Adversarial Networks. In *Computer Vision and Pattern Recognition (CVPR), 2017 IEEE Conference on*.
- Karras, T.; Aila, T.; Laine, S.; and Lehtinen, J. 2017. Progressive growing of gans for improved quality, stability, and variation. *arXiv preprint arXiv:1710.10196*.
- Karras, T.; Laine, S.; and Aila, T. 2019. A style-based generator architecture for generative adversarial networks. In *Proceedings of the IEEE/CVF Conference on Computer Vision and Pattern Recognition*, 4401–4410.
- Khandelwal, U.; Levy, O.; Jurafsky, D.; Zettlemoyer, L.; and Lewis, M. 2019. Generalization through memorization: Nearest neighbor language models. *arXiv preprint arXiv:1911.00172*.
- Kingma, D. P.; and Welling, M. 2013. Auto-encoding variational bayes. *arXiv preprint arXiv:1312.6114*.
- Leśniak, D.; Sieradzki, I.; and Podolak, I. 2018. Distribution-Interpolation Trade off in Generative Models. In *International Conference on Learning Representations*.
- Li, C.; Zhu, J.; and Zhang, B. 2016. Learning to Generate with Memory. In *Proceedings of The 33rd International Conference on Machine Learning*, volume 48 of *Proceedings of Machine Learning Research*, 1177–1186. New York, New York, USA: PMLR.
- Liu, Z.; Luo, P.; Wang, X.; and Tang, X. 2015. Deep Learning Face Attributes in the Wild. In *Proceedings of International Conference on Computer Vision (ICCV)*.
- Makhzani, A.; Shlens, J.; Jaitly, N.; and Goodfellow, I. J. 2016. Adversarial autoencoders. In *Proc. ICLR*.
- Mescheder, L.; Nowozin, S.; and Geiger, A. 2017. Adversarial Variational Bayes: Unifying Variational Autoencoders and Generative Adversarial Networks. In *International Conference on Machine Learning (ICML)*.
- Mescheder, L.; Nowozin, S.; and Geiger, A. 2018. Which Training Methods for GANs do actually Converge? In *International Conference on Machine Learning (ICML)*.
- Netzer, Y.; Wang, T.; Coates, A.; Bissacco, A.; Wu, B.; and Ng, A. Y. 2011. Reading Digits in Natural Images with Unsupervised Feature Learning. In *NIPS Workshop on Deep Learning and Unsupervised Feature Learning 2011*.
- Norouzi, S.; Fleet, D. J.; and Norouzi, M. 2020. Exemplar VAE: Linking Generative Models, Nearest Neighbor Retrieval, and Data Augmentation. In Larochelle, H.; Ranzato, M.; Hadsell, R.; Balcan, M. F.; and Lin, H., eds., *Advances in Neural Information Processing Systems*, volume 33, 8753–8764. Curran Associates, Inc.



Parzen, E. 1962. On Estimation of a Probability Density Function and Mode. *The Annals of Mathematical Statistics*, 33(3): 1065 – 1076.

Rezende, D.; and Mohamed, S. 2015. Variational Inference with Normalizing Flows. In Bach, F.; and Blei, D., eds., *Proceedings of the 32nd International Conference on Machine Learning*, volume 37 of *Proceedings of Machine Learning Research*, 1530–1538. Lille, France: PMLR.

Rubanova, Y.; Chen, R. T.; and Duvenaud, D. K. 2019. Latent ODEs for irregularly-sampled time series. *Advances in neural information processing systems*.

Singh, R.; Turaga, P.; Jayasuriya, S.; Garg, R.; and Braun, M. 2019. Non-Parametric Priors For Generative Adversarial Networks. In *International Conference on Machine Learning*, 5838–5847. PMLR.

Tomczak, J.; and Welling, M. 2018a. VAE with a Vamp-Prior. In *Proceedings of the Twenty-First International Conference on Artificial Intelligence and Statistics*, volume 84 of *Proceedings of Machine Learning Research*, 1214–1223. PMLR.

Tomczak, J.; and Welling, M. 2018b. VAE with a Vamp-Prior. In *International Conference on Artificial Intelligence and Statistics*, 1214–1223. PMLR.

Tulyakov, S.; Liu, M.-Y.; Yang, X.; and Kautz, J. 2018. Mocogan: Decomposing motion and content for video generation. In *Proceedings of the IEEE conference on computer vision and pattern recognition*, 1526–1535.

Ulyanov, D.; Vedaldi, A.; and Lempitsky, V. 2018. It Takes (Only) Two: Adversarial Generator-Encoder Networks. In *AAAI Conference on Artificial Intelligence*.

White, T. 2016. Sampling Generative Networks. arXiv:1609.04468.

Yildiz, C.; Heinonen, M.; and Lahdesmaki, H. 2019. Ode2vae: Deep generative second order odes with bayesian neural networks. In *Advances in Neural Information Processing Systems*, 13412–13421.

Zhang, H.; Gao, X.; Unterman, J.; and Arodz, T. 2020. Approximation capabilities of neural ODEs and invertible residual networks. *International conference on machine learning*.

Zhu, J.-Y.; Park, T.; Isola, P.; and Efros, A. A. 2017. Unpaired Image-to-Image Translation using Cycle-Consistent Adversarial Networks. In *Computer Vision (ICCV), 2017 IEEE International Conference on*.

## Architecture and Setup

For our baselines and the proposed model, we borrow the architecture for generator and discriminator from PGAN (Karras et al. 2017). For ALI, following (Dumoulin et al. 2016), we use two networks  $D_{\mathcal{X}}$  and  $D_{\mathcal{Z}}$  to extract features from a given image  $X$  and latent vector  $Z$  respectively which are subsequently concatenated and passed through a joint network  $D_{\mathcal{X},\mathcal{Z}}$  to obtain  $D(X, Z)$ . To ensure fairness, all models were trained progressively. The encoder  $E$ 's architecture uses the same layers as the first 12 layers of the discriminator architecture's  $D_{\mathcal{X}}$  component.

For NeurInt, the position Encoder  $E$  and velocity encoder  $\mathcal{V} = (\mu_{\mathbf{v}}, \sigma_{\mathbf{v}})$  are both one hidden layer MLPs with a LeakyReLU nonlinearity, and the vector field  $f$  of the Second Neural ODE is a 2 layer MLP with a tanh nonlinearity. The relative weighting hyperparameter  $\lambda$  in the loss for NeurInt was decayed linearly from 1000 to 100 per half cycle of each progressive step and then kept stable at 100 for the next half-cycle of the step.

To maintain consistency, we also trained the encoder  $E_P$  for PGAN by growing it progressively. We obtained an RMSE error of 0.0522 on the held-out test set upon training. Figure 6 shows some reconstructions on held-out test data which qualitatively indicate the convergence of the encoder.

We use the same optimizer for PGAN and NeurInt as proposed in (Karras et al. 2017) and for ALI as in (Dumoulin et al. 2016).

For all our experiments, we use 2 Nvidia GeForce GTX 1080 Ti GPUs.

## FID Statistics

Using the training set as the support, we compute the FID scores of NeurInt and our baselines (using the same procedure as described in the main paper), over 100 randomized runs, and report the mean and standard deviation of the FID scores obtained in Table 7.

## Additional Samples

**Interpolation Samples :** Figures 7 and 8 qualitatively demonstrate NeurInt's ability to generate significantly more realistic and smoother interpolation trajectories over the baselines.

**Uncurated Samples :** Figure 9 shows uncurated samples from NeurInt and baselines. The quality of the generated samples of NeurInt against the baselines backs up the superior FID achieved by NeurInt. This demonstrates NeurInt to be not only a good interpolation methodology but also a good generative model.

**Distribution of trajectories :** Figure 10 demonstrates qualitatively NeurInt's ability to draw interpolations from a distribution of interpolation trajectories. Particularly note the transition between a female source and male target with different facial attributes.

**Ablation Study :** Figure 11 demonstrates the benefits of our joint training mechanism, with NeurInt interpolation trajectory being of significantly better quality than NeurInt-PT.

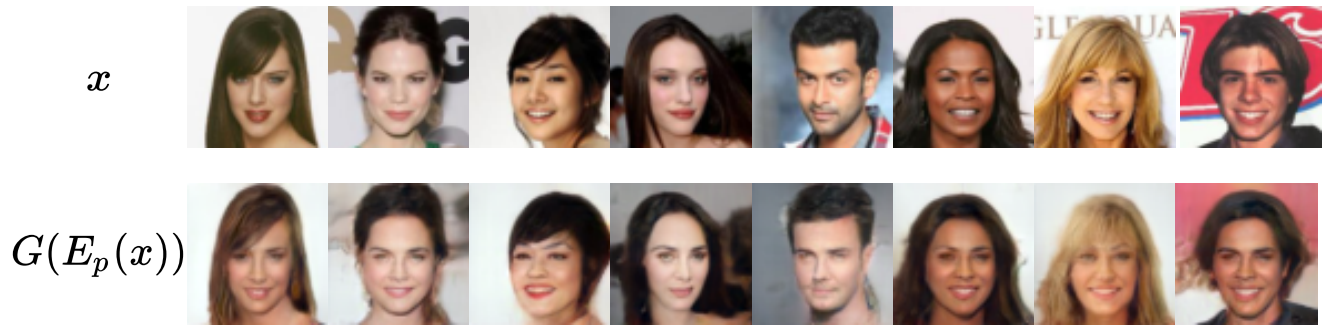


Figure 6: Sample Reconstructions of Encoder  $E_p$

Table 7: FID Score Statistics for NeurInt, PGAN and ALI on CelebA and SVHN. Lower FID is better. For all sampling methods other than PRIOR, the training set is used as the support

DATASET	METHOD	PGAN	ALI	NEURINT
SVHN	PRIOR	17.05±0.082	46.45±0.075	
	LERP	25.23±0.072	36.59±0.073	<b>6.45±0.069</b>
	SLERP	25.43±0.081	36.52±0.066	
CELEBA	PRIOR	11.57±0.088	19.25±0.085	
	LERP	36.29±0.078	24.20±0.090	<b>10.22±0.082</b>
	SLERP	36.44±0.081	24.25±0.091	



Figure 7: Comparison of Interpolation quality between PGAN, ALI and NeurInt on the CelebA dataset.  $x_S$  (leftmost) and  $x_T$  (rightmost) denote the true source-target pair from the training set on which the trajectory was conditioned. The interpolation trajectories (shown in the middle) begin at  $\tilde{x}_S$  (reconstruction of  $x_S$ ) and end at  $\tilde{x}_T$  (reconstruction of  $x_T$ )

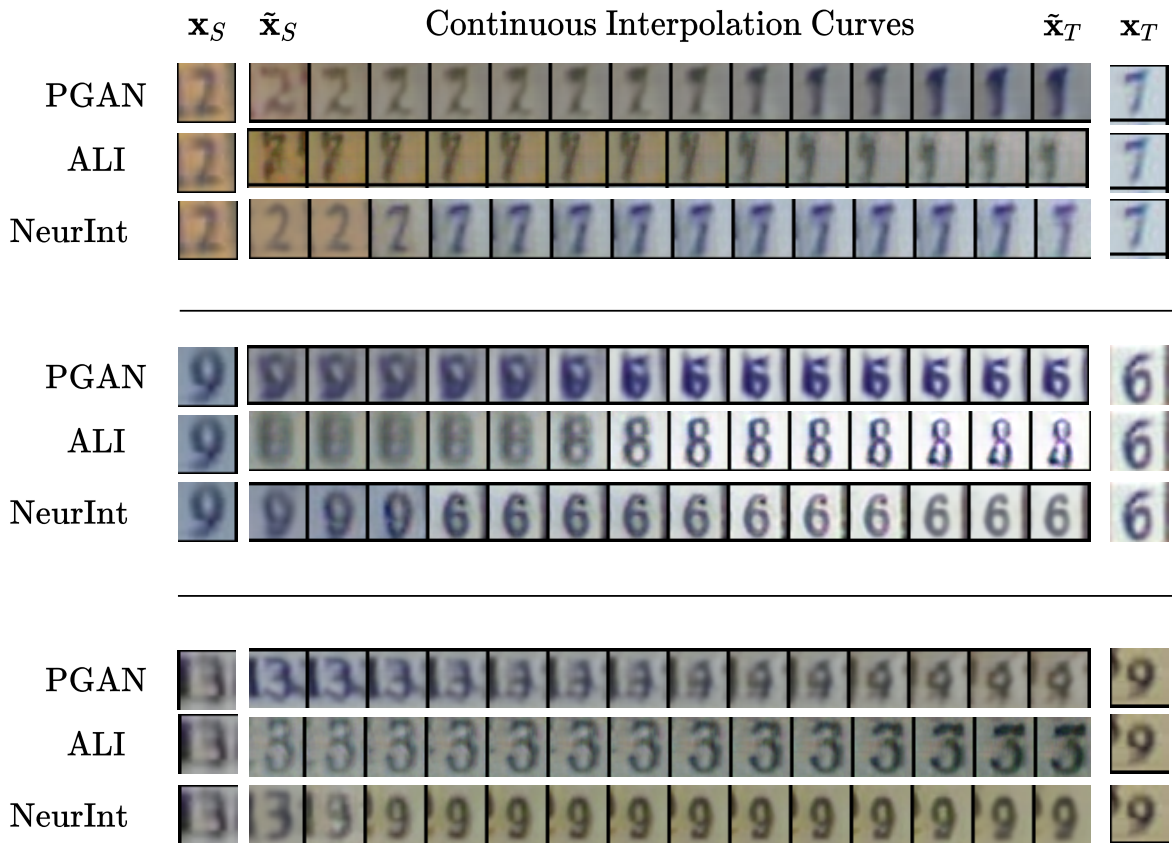


Figure 8: Comparison of Interpolation quality between PGAN, ALI and NeurInt on the SVHN dataset.  $\mathbf{x}_S$  (leftmost) and  $\mathbf{x}_T$  (rightmost) denote the true source-target pair from the training set on which the trajectory was conditioned. The interpolation trajectories (shown in the middle) begin at  $\tilde{\mathbf{x}}_S$  (reconstruction of  $\mathbf{x}_S$ ) and end at  $\tilde{\mathbf{x}}_T$  (reconstruction of  $\mathbf{x}_T$ )



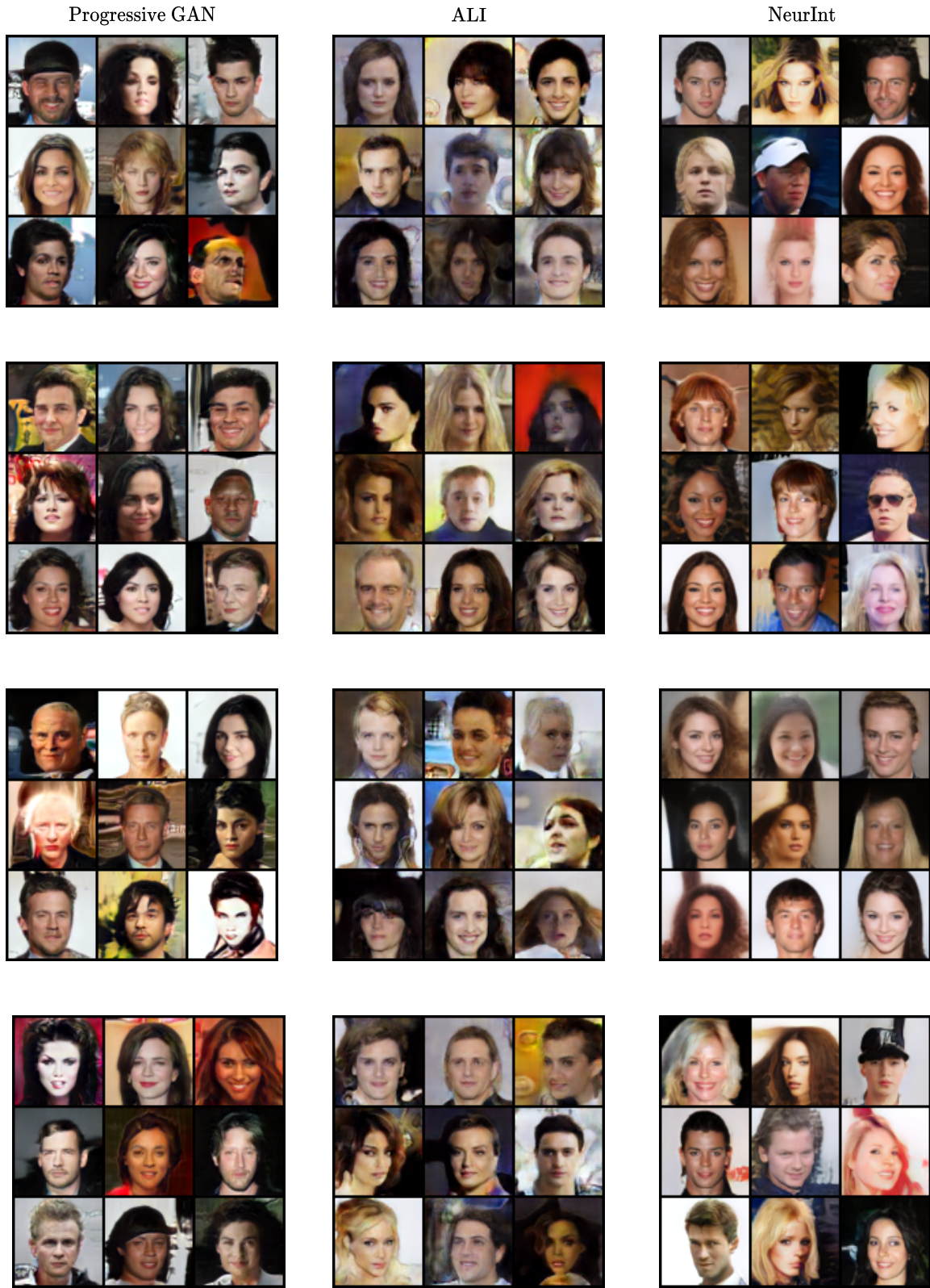


Figure 9: Uncurated samples from Progressive GAN (left), ALI (middle), and NeurInt (right) trained on the CelebA dataset. Samples from Progressive GAN and ALI are drawn from their true prior distribution, whereas samples from NeurInt are drawn by first generating continuous-time trajectories and then evaluating them at random intermediate points



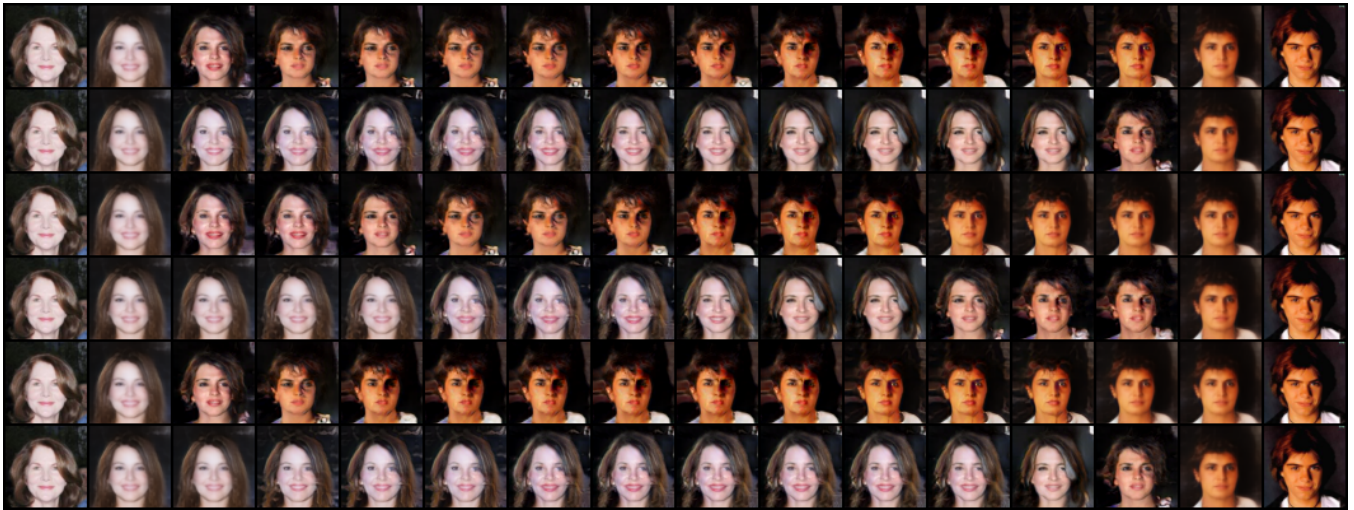
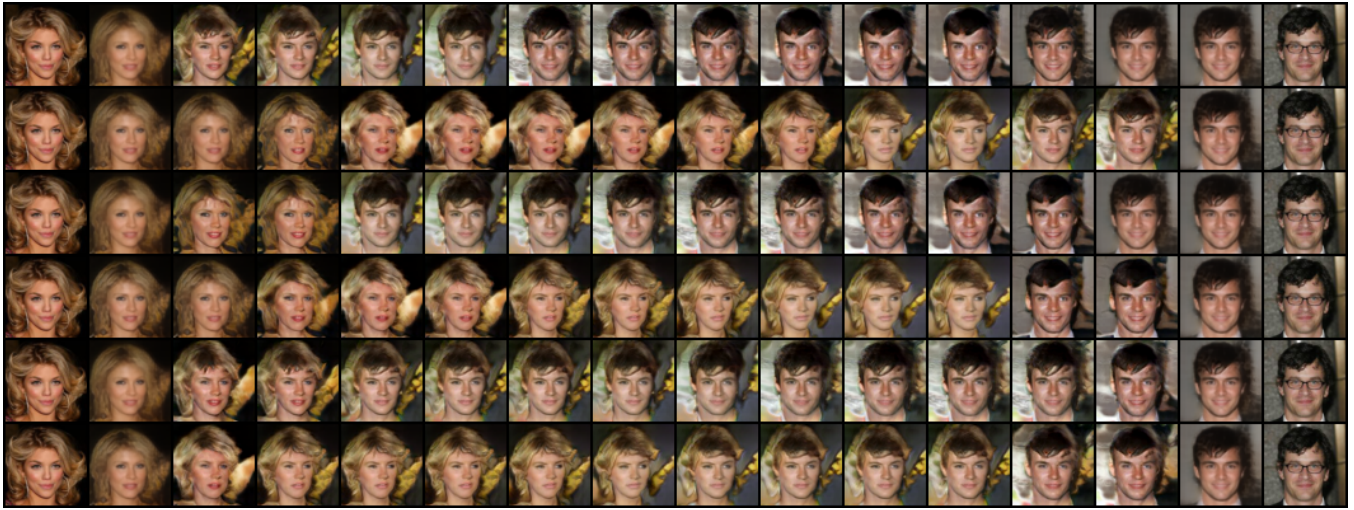


Figure 10: NeurInt’s samples upon choosing different random initial velocities demonstrating the model’s ability to learn a distribution of trajectories. Each row is an interpolation between the real images on the first and last columns.

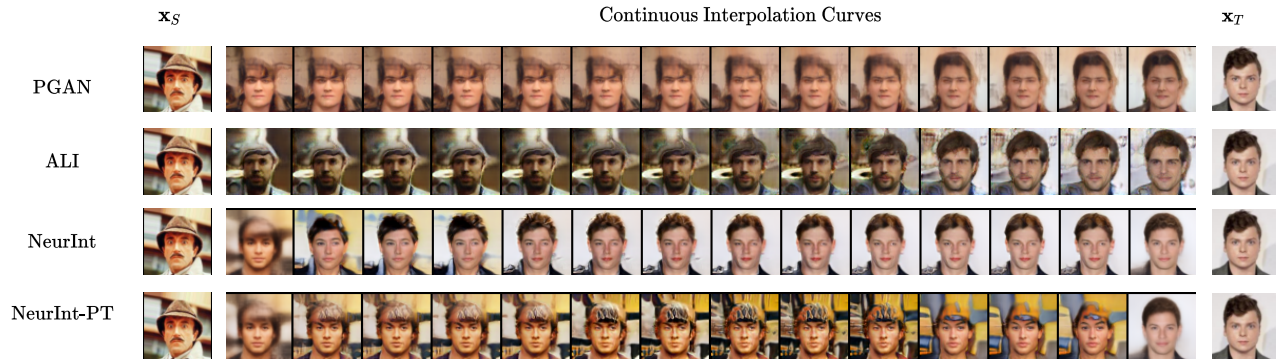


Figure 11: Example Interpolations for PGAN, ALI, NeurInt and NeurInt-PT. The first and last columns contain the source and target images respectively